

Chapter 7

Ferroelectricity in Halide Perovskites

HOLGER RÖHM

Abstract

Classic ferroelectrics are mostly oxide perovskites, some of which have been discussed in the previous chapters. The counterparts, halide perovskites, usually possess semiconducting and ionic conducting properties and thus examining the potential ferroelectricity is complicated. The susceptibility to degradation also impedes or limits many established characterization techniques known from ceramic ferroelectrics. These factors have contributed to the controversy in the scientific community regarding ferroelectricity in halide perovskites. This chapter provides an overview on the material class of halide perovskites, their novel applications in thin film solar cells, and how ferroelectricity affects their properties. Novel measurement approaches reveal material properties related to ferroelectricity, providing not only insights into the working principles of halide perovskite devices but also hint towards pitfalls for common characterization techniques.

7.1 The rise of halide perovskites and their applications

7.1.1 Halide perovskites

Halide Perovskites can refer to a multitude of crystalline compounds, yet in recent years this term is often used synonymously for a class of organic or inorganic metal halides with semiconducting properties. These materials have found a variety of applications in optoelectronics, particularly in photovoltaics (Green *et al.*, 2014). In 2006, Kojima *et al.* for the first time reported the use of methylammonium lead bromide as a light absorber in dye sensitized solar cells (Kojima *et al.*, 2006). While these initial devices were only short lived, their promising power conversion efficiency (PCE) of 2.2 % soon lead to the discovery of solid state solar cells that no longer required any liquid electrolyte hence marking the birth of what is nowadays known as perovskite solar cells (Lee *et al.* 2012; Kim *et al.*, 2012).

Within halide perovskite semiconductors, we can differentiate between three general types based on the A-site cation of the ABX_3 structure while all three types mainly utilise Pb or Sn at the B site, and Br, Cl or I on the X site:

- (1) Organic metal halide (OMH) perovskites, which contain a small cation molecule at the A-site,
- (2) Inorganic metal halides (IMH) most often comprising Cs at the A-site of the crystal and,
- (3) Solid solutions of types (1) and (2).

The most common A-site cations used in OMH perovskites are methylammonium (MA) and formamidinium (FA) while small amounts of other similarly sized cation molecules can be tolerated by the crystal lattice (Hsieh *et al.*, 2017; Wang *et al.*, 2017a). There is an ongoing discussion whether these dipolar organic molecules are in fact required for the superb electronic properties that allowed these materials to facilitate thin film solar cells with PCEs beyond 25 %. Some simulations suggested that alignment of these dipoles could influence photogenerated free charge carriers while others rather concluded minimal or no influence (Frost and Walsh, 2016; Pecchia *et al.*, 2015; Wilson *et al.*, 2019). One of the main reasons for the multitude of optoelectronic applications of halide perovskites are their long-lived electronic charge carriers based on low nonradiative recombination rates that minimize thermal losses. These properties would not be unusual in perfect single crystalline materials as is known from Si or GaAs, but halide perovskites provide these properties in polycrystalline thin films that are commonly deposited from precursor solutions and therefore comprise high defect densities (Wang *et al.*, 2018; Ono *et al.*, 2019).

Generally, both organic molecules and halides limit the temperature stability of halide perovskites hence driving the search for new compositions. So far, both inorganic and organic halide perovskites could not reach the same PCEs in solar cells unless a significant portion of the A-site comprised either MA or FA molecules, the B site comprised mostly Pb^{2+} ions and the X site comprised Br, Cl or I (Tai *et al.*, 2019; Chen *et al.*, 2021). Fig. 7.1 contains an overview on the band gaps as well as valence and conduction band energies of the most common metal halide compositions.

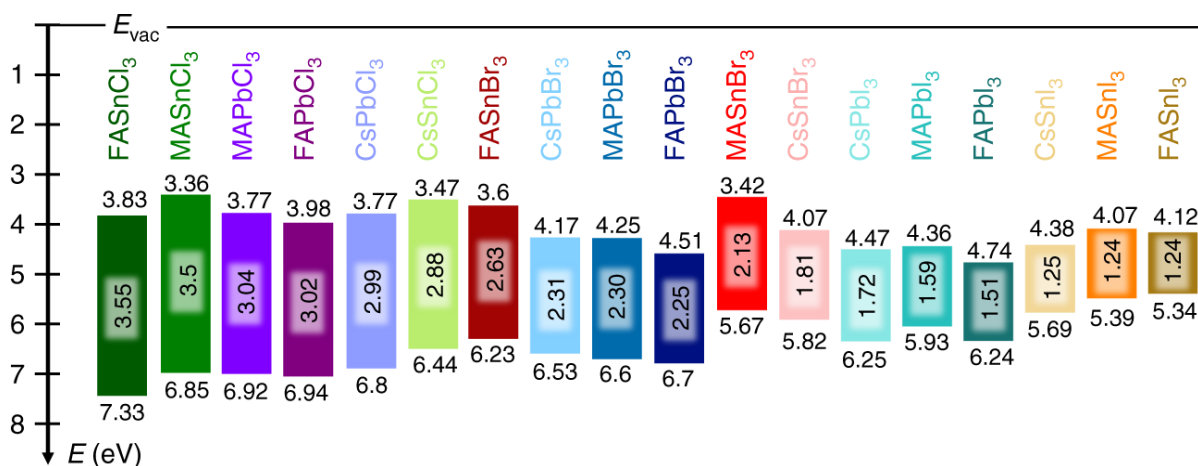


Figure 7.1. Compositional range for band gap tuning of halide perovskites using Cs^+ , FA^+ and MA^+ as an A-site cation, Pb^{2+} or Sn^{2+} as a B-site cation and Br, Cl or I as an X-site anion. (Reproduced according to CC BY-SA 4.0, Tao *et al.*, 2019.)

In order to tune the optical and electronic properties of halide perovskites and to increase their long-term stability, the use of solid solutions became a common approach. This approach allows design of halide perovskite materials with a band gap ranging from 1.1 eV up to 4.5 eV. This is pivotal for tandem solar cells, where a wide bandgap solar cell is combined with a small bandgap solar cell in order to overcome the Shockley-Queisser limit for single junction solar cells and thereby enables PCEs of above 33 %. Furthermore,

changing the bandgap enables colour tuning for light emitting devices. Currently, most high PCE perovskite solar cells use solid solutions of (Cs,FA,MA)₃Pb(I,Br) with small concentrations (<20 mol.%) of Cs and Br (Saliba *et al.*, 2016; Yoo *et al.*, 2021). Besides the aforementioned regular 3D perovskite structures, the use of 2D or 1D perovskites turned out to provide a wide range of material properties, particularly used as interface modification for 3D perovskite absorbers (Chao *et al.*, 2018).

7.1.2 Common applications for halide perovskites

The first major application for halide perovskite semiconductors was their use as light absorbing “active” material in solar cells that led to their rise within the global research community. Based on their optoelectronic properties such as the sharp absorption/emission onset, a direct bandgap reaching from the visible range down to the near infrared (Fig. 7.1), long lifetimes of excited charge carriers, as well as ease of fabrication from simple salt precursor solutions, halide perovskites quickly found use in other applications. Closely related to solar cells, halide perovskite photodetectors make use of the unique optoelectronic properties and in particular can allow for colour sensitive detection based on the tuneable band gap via the aforementioned compositional engineering. The inverse process of light absorption and the conversion of a photon’s energy into excited charge carriers in a semiconductor’s conduction band is light emission by radiative recombination. This process allows the use of halide perovskites in perovskite light emitting devices (P-LEDs) and perovskite lasers (Veldhuis *et al.*, 2016). In order to obtain light emission with an even narrower emission peak, researchers successfully produced halide perovskite quantum dots (Wang *et al.*, 2017b). Another application that has been explored with halide perovskites is X-ray detection. Since OMH perovskites contain halides with high electron densities as well as Pb or Sn, the absorption coefficient of these crystals is sufficiently high in order to allow a high photon absorption coefficient and sensitivity for X-rays. The excited charge carriers far exceed the band gap energy of these perovskites and after relaxation to the band edges the increased conductivity can be detected by drift current measurements (Wei and Huang, 2019).

7.2 Controversy around ferroelectricity in methylammonium lead iodide

In 2014, Frost *et al.* proposed the concept that light-absorbing semiconductors which also exhibit spontaneous ferroelectric polarization might exhibit favourable electronic properties for photovoltaic applications and, that methylammonium lead iodide (MAPbI₃) might indeed be such a material (Frost *et al.*, 2014). They concluded that a semiconducting ferroelectric that spontaneously forms domains of alternating polarization could lead to reduced Shockley Read Hall (SRH) recombination. Yet, at that time, there was no experimental proof for ferroelectricity in halide perovskites and this model was mainly based on simulations and theoretical considerations. Later in 2014, Kutes *et al.* reported the observation of ferroelectric domains in MAPbI₃ via piezoresponse force microscopy (PFM) but they did not observe ordered domains which typically form in classic ferroelectrics (Kutes *et al.*, 2014). In 2016 and 2017 two following reports by Hermes *et al.* and Röhm *et al.* revealed highly ordered domain structures in MAPbI₃, as shown in Fig. 7.2a and b (Hermes *et al.*, 2016, Röhm *et al.*, 2017).

Hermes *et al.* assigned these domains to ferroelasticity since ferroelectric poling could not be readily observed in this material, while Röhme *et al.* concluded that the domains are ferroelectric based on their alternating piezoresponse and their effect on charge carrier extraction in conductive atomic force microscopy (AFM) measurements. In the following years, multiple studies investigated the nature of these domains with seemingly contradictory results. Liu *et al.* showed that the surface of domains in MAPbI₃ sometimes exhibit a chemical contrast of methylammonium concentration. They assigned this effect to ferroelastic twinning and concluded that this chemical segregation is the reason for a contrast in PFM measurements (Liu *et al.*, 2018). In particular, they pointed out that the use of signal amplification near the contact resonance frequency of the AFM cantilever makes the signal susceptible to misinterpretation. This study also observed the same twin domains in band-excited PFM, yet Liu *et al.* pointed out that this could be due to local contact resonance variations that might be caused by ferroelastic strain. In a response, Schulz *et al.* argued that these effects are not contradictory to ferroelectricity since all ferroelectrics are also ferroelastic due to their non-centrosymmetry and that a chemical contrast via screening ions at the surface of such domains is in fact to be expected (Schulz *et al.*, 2019). Nevertheless, both viewpoints were supported by valid arguments which kept the discussion open (Liu *et al.*, 2019).

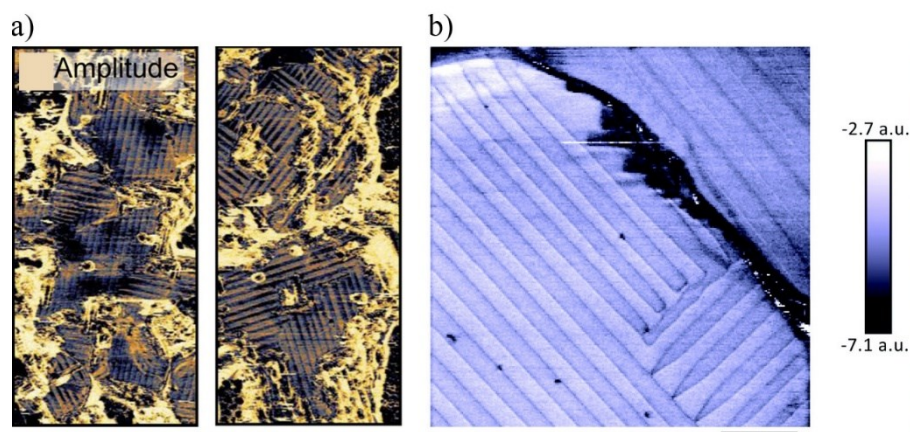


Figure 7.2. (a) PFM amplitude image of a MAPbI₃ sample by Weber *et al.* assigned to ferroelastic twinning. (Adapted with permission from Hermes, I. M. *et al.* (2016) Ferroelastic Fingerprints in Methylammonium Lead Iodide Perovskite, *J. Phys. Chem. C*, 120(10), pp. 5724-5731. Copyright 2016 American Chemical Society. (b) PFM inphase image of MAPbI₃ by Röhme *et al.* claiming ferroelectric properties. (Scale bar 360 nm. Adapted from Ref. Röhme *et al.*, 2017 with permission from the Royal Society of Chemistry.)

One particular property of MAPbI₃ solar cells that was initially suspected to be caused by ferroelectricity is a hysteresis in current-density-voltage (JV) sweeps (Wei *et al.*, 2014). Yet, as it turned out, this hysteresis is mainly related to changes of ionic charge carrier accumulation or depletion at interfaces between the perovskite film and charge carrier transport or electrode layers (Weber *et al.*, 2018). Although ferroelectric domains and ferroelectric poling could influence these properties as well, the majority of the observed hysteresis effects are likely not caused by ferroelectric poling. Leguy *et al.* argued that based on Monte Carlo simulations, the timescales of ferroelectric switching, if related to the alignment of MA⁺ dipole molecules, would be on the order of 1 ms and hence faster than the experimentally observed effects in perovskite solar cells (Leguy *et al.*, 2015). This conclusion is in line with the observation of similar JV-hysteresis in metal halide perovskites that possess a centrosymmetric cubic structure and hence a paraelectric crystal phase at room

temperature such as FAPbI₃ and MAPbBr₃.

The crystal structure and hence the space group of all halide perovskites is decisive for the possibility for, or exclusion of, ferroic properties. To date, some uncertainty remains regarding the allocation of space groups for some compounds. This is often based on limitations to the accuracy of diffraction methods since even tiny offsets in the atomic positions in the crystal lattice can make the difference between macroscopically polar and nonpolar materials (Richter *et al.*, 2018). For archetypical MAPbI₃ and similar metal halides, instability under irradiation and a significant amount of dynamic disorder at elevated temperatures further complicate these measurements (Poglitsch and Weber, 1987). Breternitz *et al.* recently showed that an offset of iodine atoms in the crystal lattice supports the allocation of the non-centrosymmetric and even polar tetragonal space group I4cm for MAPbI₃, which is a prerequisite for ferroelectricity (Breternitz *et al.*, 2019; Breternitz *et al.*, 2020). At higher temperatures (>327 K), MAPbI₃ presents itself in the cubic and thereby paraelectric space group Pm $\bar{3}$ m (Poglitsch and Weber, 1987). The phase transition temperature is very close to room temperature, which not only indicates a low energetical difference between the tetragonal and cubic crystal symmetry as pointed out by Breternitz *et al.*, but this also requires careful temperature control during commonly employed X-ray diffraction (XRD) measurements on this material. Unless conducted under temperature-controlled conditions, these measurements can be distorted by local heat sources such as illumination or environmental influences, which could unintentionally lead to measurements close to or above the Curie temperature (T_C) and thereby skew the results.

One of the biggest concerns in the discussion about the nature of the previously reported domain structures in MAPbI₃ is the lack of saturating polarization (P)-electric field (E) ferroelectric hysteresis loops (PE loops) as one of the hallmarks for ferroelectricity. Whenever an electric field is applied to a MAPbI₃ sample, a current composed of free electronic charge carriers and mobile ions is driven through the crystal. Besides the thermally activated electrons and holes, any above bandgap (> 1.6 eV) photon illumination further increases the charge carrier density and thereby the sample's conductivity. The ionic currents are temperature dependent with relatively low activation energies of ~0.29 eV and ~0.9 eV for I⁻ and MA⁺ respectively (Futscher *et al.*, 2019). The resulting overall conductivity leads to thermal damage to MAPbI₃ samples even at moderate electric poling fields on the order of 5 V/μm. Fig. 7.3a depicts a PE-curve of a perovskite thin film sample in a typical solar cell architecture. Even at small electric fields of 1.5 V/μm, a current occurs that quickly rises and does not reach saturation before thermal destruction occurs. This can be avoided by limiting the electric field to approximately 3.0 V/μm, but mainly capacitive behaviour with a significant leakage (ohmic/shunt) component can be observed in the resulting PE-curve. In contrast, classic insulating ferroelectrics such as BiFeO₃ retain a very small current up to ~20 V/μm before ferroelectric switching mediates a poling current (Fig. 7.3b).

In order to limit ionic contributions to the leakage current of MAPbI₃, Rakita *et al.* cooled samples to 204 K and observed a saturation in the complex part of the dielectric response during AC poling experiments (Rakita *et al.*, 2017). Compared to ceramic ferroelectrics, in MAPbI₃ thermal degradation sets in at comparatively low temperatures of ~420 K, limiting the maximum current density in poling experiments (Kim *et al.*, 2018a). Additionally, thin film samples in solar-cell architectures (Fig 7.3a) often show strong [110] texture hence confining the c-axis of the tetragonal crystals to an in-plane orientation parallel to the substrate and orthogonal to the electric field between electrodes (Leonhard *et al.*, 2019; Wu *et al.*, 2018). Therefore, the magnitude of the minimal electric field that might induce quick ferroelectric switching (coercive field) is increased compared to experiments where the poling field aligns with the c-axis of the crystalline sample.

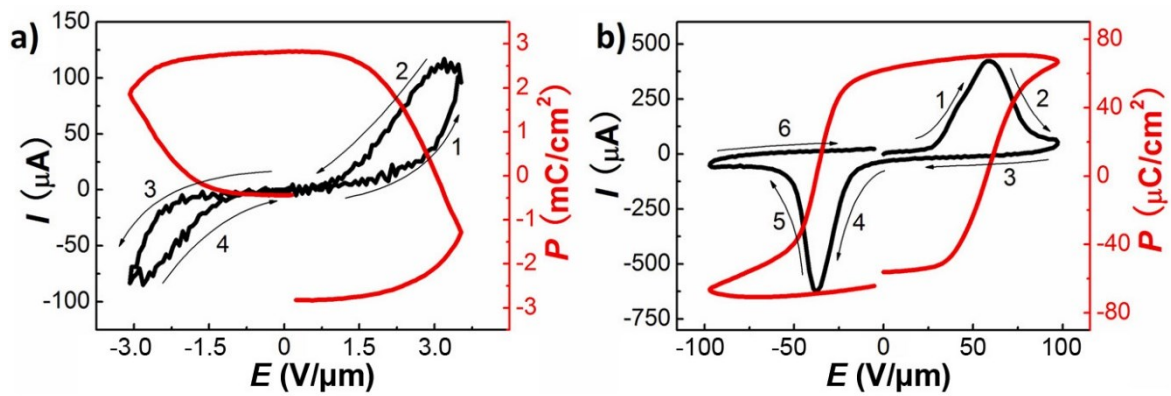


Figure 7.3. (a) Polarization curve of an ITO/PEDOT:PSS/MAPbI₃/Au thin film sample (10 Hz) that does show semiconducting and capacitive behaviour unlike classic insulating ferroelectric samples. (b) Reference measurement of a ferroelectric capacitor of Au/BiFeO₃/SrRuO (1000 Hz) showing clear saturation of the polarization curve. (Adapted with permission from Fan, Z. et al. (2015) Ferroelectricity of CH₃NH₃PbI₃ Perovskite, *J. Phys. Chem. Lett.*, 6(7), pp. 1155-1161. Copyright 2015 American Chemical Society.)

In order to minimize the electric field that is required to achieve ferroelectric switching, Röhme *et al.* used a sample layout of interdigitated gold electrodes covered by a thin film of MAPbI₃ for ferroelectric poling experiments (Fig. 7.4a and b) (Röhme *et al.*, 2019).

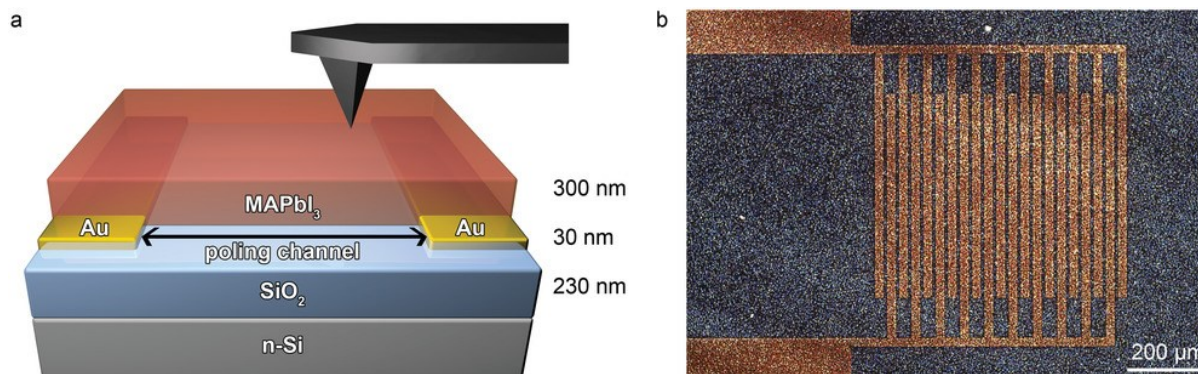


Figure 7.4. (a) Schematic of interdigitated gold electrodes atop an n-doped silicon substrate allowing the application of an in-plane poling field to the MAPbI₃ thin film and surface sampling via AFM before and after poling. The insulating SiO₂ layer prevents leakage currents through the substrate. (b) A light microscope image shows the MAPbI₃ thin film covering the electrode layout. (Reproduced according to CC BY-SA 4.0, Röhme *et al.*, 2019.)

In this configuration, the poling field between the gold electrodes lies in the same plane as the tetragonal c-axis of the [110] textured film. Since the current response of MAPbI₃ samples shows a diode-like onset behaviour (Fig. 7.3a), the minimization of the electric field maximum is key in order to prevent thermal damage to the sample due to high currents. Accordingly, application of a small electric field for an extended period of time is a promising strategy. In the past, this creeping poling was successfully used in ceramic PZT ferroelectrics in order to reduce the electric field required for ferroelectric poling (Zhukov *et al.*, 2010). The current characteristics of Röhme *et al.*'s experiment are depicted in Fig. 7.5. The pristine sample shows a symmetrical and reversible current (I)-E curve, similar to a double-Schottky diode. At a characteristic onset field (E_{on}) of ± 1.6 V/ μ m, the electric current increases exponentially, indicative of the Schottky contact at the semiconductor/metal

interface. The pronounced hysteresis is likely related to accumulation of MA^+ or I^- ions at the interfaces. In contrast, during creeping poling of the MAPbI_3 film at an electric field of $2 \text{ V}/\mu\text{m}$ for 10 minutes between the interdigitated gold electrodes, the current stays below $1 \mu\text{A}$ yet results in a dramatic change of the subsequent IE-sweep characteristic (Fig. 7.5b). The poled sample possesses a diode behaviour with a reduced onset voltage of $\sim 0.5 \text{ V}/\mu\text{m}$ and current blocking at negative bias. The poling process is fully reversible via creeping poling for several minutes with opposite polarity, resulting in mirrored diode behaviour (Fig. 7.5c). The creeping poling currents over time (Fig. 7.5d and e) reveal slow poling processes over several minutes without any signs for burnout or thermal damage to the sample.

Nevertheless, based on the aforementioned properties the contribution of ferroelectric poling currents, ionic currents and even thermal degradation of the sample is hard to disentangle in macroscopic electrical measurements in MAPbI_3 and similar metal halide perovskites hence calling for microscopic investigation of the process.

7.3 Challenges for measuring ferroelectric nanostructures in methylammonium lead iodide

Unlike most functional ceramics, OMH perovskites are rather soft materials that are susceptible to damage from mechanical forces, changes in temperature and electric or ionic currents induced by measurement instruments (Li *et al.*, 2019; Feng, 2014; Sun *et al.*, 2017). Additionally, extensive measurements on thin films of hygroscopic materials such as MAPbI_3 must be conducted under dry gas atmospheres in order to avoid decomposition.

Exertion of mechanical forces or generation of mechanical stress in the sample are a pivotal part of many ferroic characterization techniques such as dilatometry, piezoresponse measurements and mechanical profilometry. Even contact mode scanning probe microscopy such as PFM and conductive AFM, which only exhibit very small forces can lead to abrasion of OMH film surfaces. This type of measurement damage is most likely to occur when the uneven topography of a polycrystalline layer is scanned at a fast rate (Hieulle *et al.*, 2017; Leonhard *et al.*, 2019). To some extent, sample damage with scanning probe measurements can be minimized by using softer cantilevers, but this approach renders the measurements more susceptible to artifacts such as electrostatic noise (Collins *et al.*, 2019). The mapping of domains in MAPbI_3 via PFM is not only challenging because of these mechanical limitations and the relatively low durability of the samples, but since this perovskite is both semiconducting for electronic charge carriers and an ionic conductor (MA^+ , I^-), these contributions will also affect any kind of measurement that modulates an electric field in the sample. In PFM, typical excitation voltages of 1-2 V are applied to the AFM tip, which translate to electric fields of $1\text{-}10 \text{ V}/\mu\text{m}$ at several kHz through the polycrystalline thin film, depending on its thickness. To what extent the resulting movement of the AFM tip is caused by a true piezoresponse of MAPbI_3 or by electrostatic or mechanical artifacts has fired up a lively scientific discussion (Schulz *et al.*, 2019; Liu *et al.*, 2019; Colsmann *et al.*, 2020; Gomez *et al.*, 2020).

While PFM does not directly measure polarization of a potential ferroelectric material but rather its local piezoresponse, it offers the possibility to directly map piezoresponsive domains that are typically on the order of 100 nm in size in a nondestructive manner. By using a device layout with a MAPbI_3 film atop interdigitated gold electrodes on an insulated silicon substrate as shown in Fig. 7.4, PFM measurements before and after each poling experiment can reveal changes in the sample (Röhm *et al.*, 2019).

If the applied electric field affects the domains (ferroelectric poling), this can be observed

directly without the need for analysis of the macroscopic poling current. Particularly on semiconducting samples, this approach does not require the distinction between parasitic conductivity and a poling current, which is used for classic hysteresis curve analysis. Fig. 7.6 shows lateral PFM measurements of two different positions on a MAPbI₃ film in their pristine state and after creeping poling at 4.5 V/μm for 11 min.

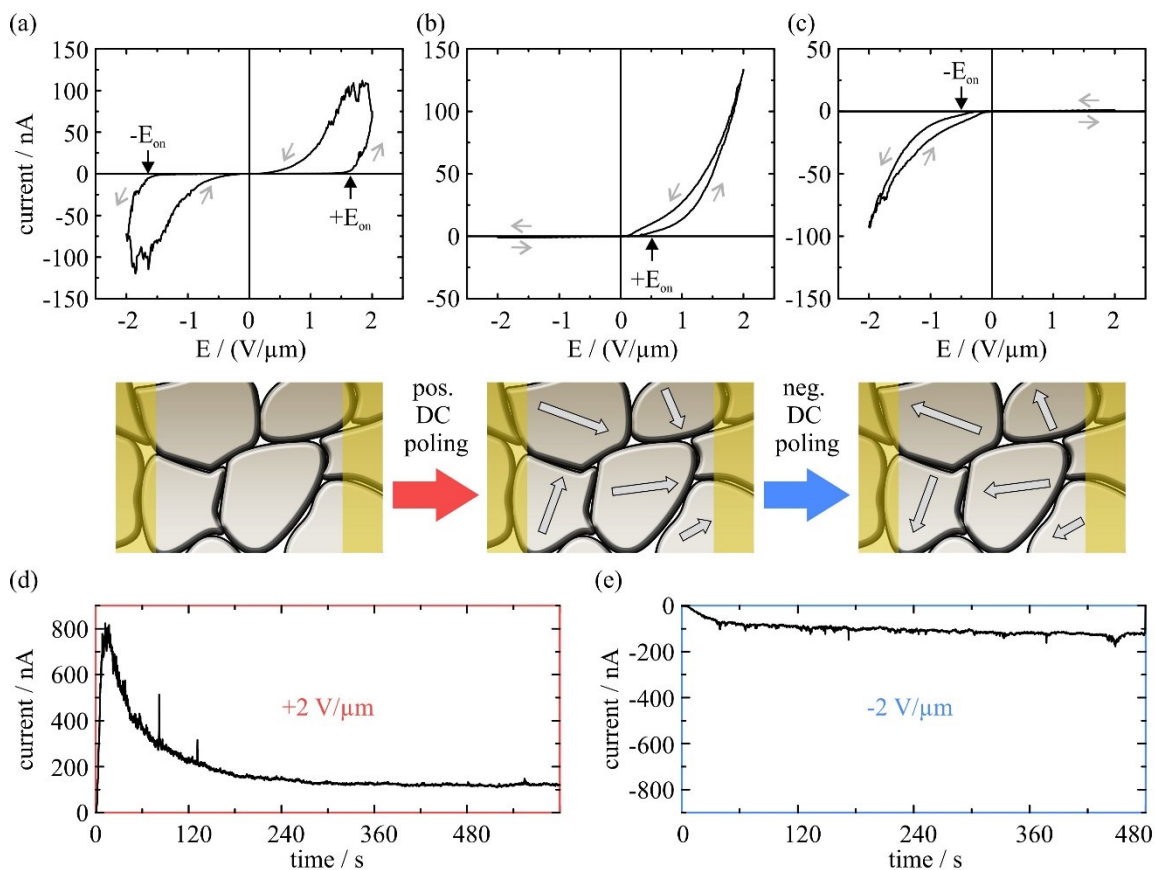


Figure 7.5. (a) Electric field sweeps between interdigitated gold electrodes result in a symmetrical double-Schottky diode behaviour of the Au/MAPbI₃/Au sample. (b) After application of an electric field of 2 V/μm for 10 minutes (creeping poling), the electrical conductivity of the device becomes directional, indicating a stable polarization of the MAPbI₃ film. (c) The directional behaviour can be inverted by application of an inverted poling field for several minutes. (d),(e) The device current gives insight into the changes of sample conductivity during creeping poling. After initial poling of the pristine sample, the sample current reaches a stable magnitude of ±120 nA for both poling directions. (Reproduced according to CC BY-SA 4.0, Röhm, 2019.)

Some clear changes in the domain patterns become apparent after poling. Not only do positions of the domain walls shift due to electric poling, but also the ratio of both types of domains within grains is altered (Fig. 7.6d and e). Generally, it is challenging to deduce the polarization direction of ferroelectric domains via PFM, but the combination of a well-known electrical poling field, the changes of domains before and after poling and the assumption of 90° domain walls based on the crystal structure allows for general conclusions on the polarization direction in this experiment (arrows in Fig. 7.6d and e). Since neighbouring domains show a clear contrast in lateral PFM amplitude, 180° domains can be ruled out (Röhm *et al.*, 2017).

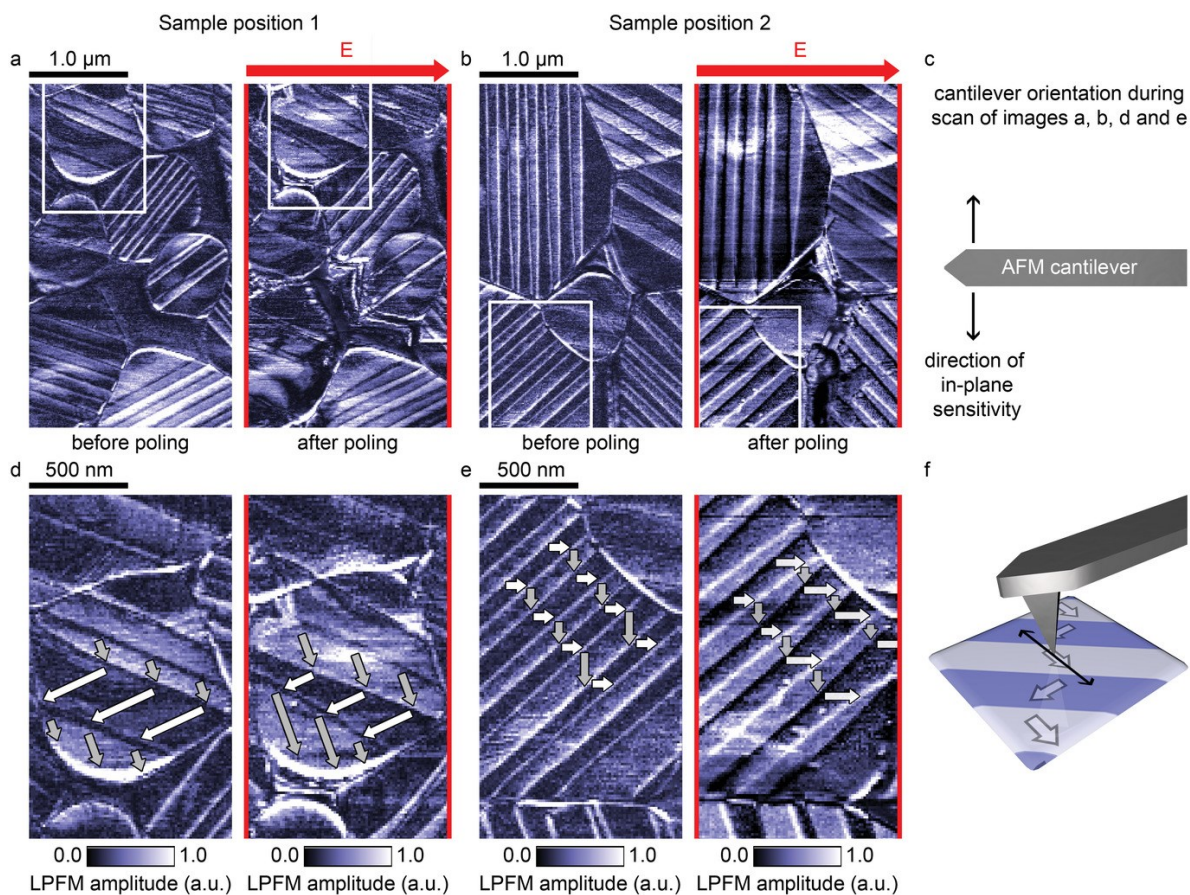


Figure 7.6. (a) Lateral PFM images of MAPbI₃ grains atop a silicon substrate (see Fig. 7.4a). The domain pattern of the pristine sample (left) changes drastically after application of DC (direct current) poling field (red markings, 4.5 V/μm, 11 min). (b) At a different sample position widening of domains with a low lateral piezoresponse (dark) can be observed after poling while domains with a high lateral piezoresponse (light blue) shrink in size. By combining these results with the orientation of the electric poling field (red arrows) and the direction of the AFM cantilever during the measurement (c), a probable configuration of domain polarization can be deduced (d-f). (Reproduced according to CC BY-SA 4.0, Röhm et al., 2019.)

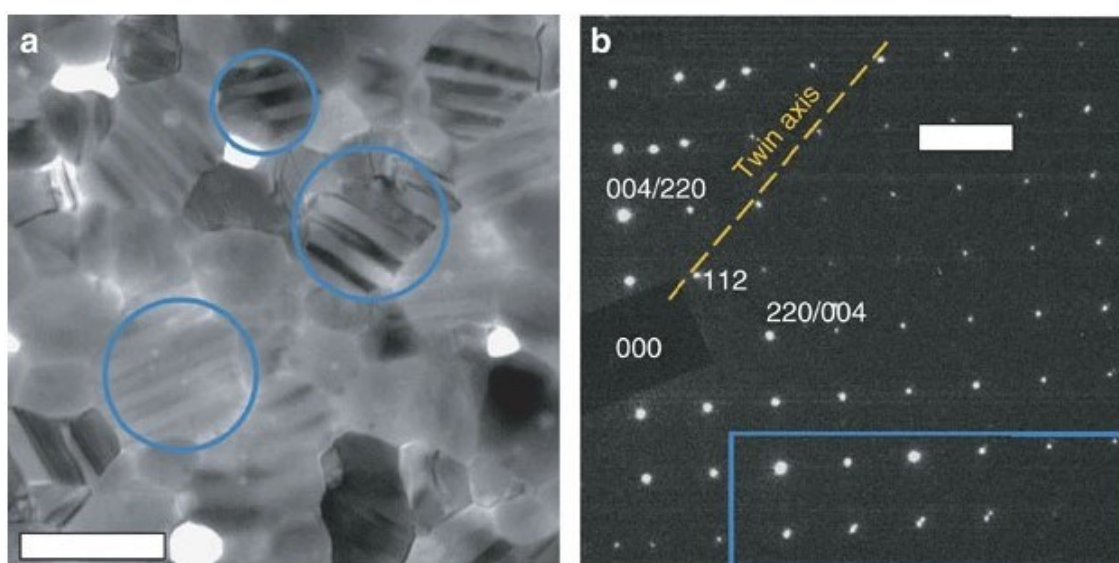


Figure 7.7. a) Bright-field TEM image of MAPbI₃ grains show a clear contrast of neighbouring domains (Scale bar 500 nm). b) Diffraction pattern taken from a grain exhibiting stripe contrast (scale bar 2/nm). (Reproduced according to CC BY-SA 4.0, Rothmann et al., 2017b.)

Besides PFM, scanning electron microscopy (SEM) or scanning transmission electron microscopy (STEM) are techniques that can reveal ferroelectric domains and even crystal lattice resolution of the atomic and molecular arrangement within crystals, as shown in Fig. 7.7. However, they require carefully chosen measurement parameters in order to avoid damage to the sample especially in metal halide perovskites. The most common issue is direct beam damage where the beam of accelerated electrons degrades the perovskite (Rothmann *et al.*, 2017a). Both the acceleration voltage (energy per electron) and the beam current (rate of electron incidence) have to be within a certain range in order to obtain a sufficient measurement signal from the detectors as well as to correlate the signal with energy input into the specimen, as explained in Fig. 7.8. In particular, not only OMH perovskites are susceptible to decomposition of the organic compound due to this energy influx and resulting heating and ionization, but also inorganic metal halides such as CsPbI₃ can be damaged, even though they show more resilience (Xiao *et al.*, 2015).

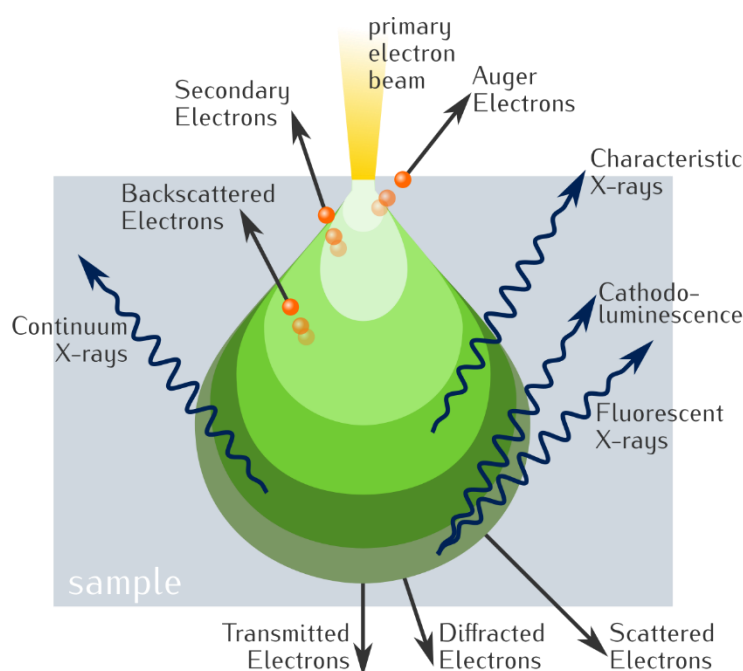


Figure 7.8. Overview for interactions of an electron beam with a sample. Depending on the type of interaction, the measurement can introduce significant degradation to the sample, limiting the measurement duration and other measurement parameters when probing OMH perovskites. (image credit: Wikipedia user Ponor, distributed under CC BY-SA 4.0.)

Resolving crystal orientation with sub-grain resolution in samples with micrometer sized grains is often required in order to link measurement results from other microscopy techniques such as PFM to the crystal lattice. Electron backscatter diffraction (EBSD) which is based on SEM is one of the few microscopy techniques that can provide this information in a non-destructive manner. In EBSD, the electron beam of an SEM is probing the sample surface at an angle of 20° and the resulting Bragg-diffraction pattern is measured on a detector screen. This interference pattern is then matched to a crystallographic orientation based on the appropriate space group. This software-based matching requires a sufficient signal amplitude in the detector and a signal contrast that can be matched to simulated patterns. In OMH perovskites, the duration of electron beam irradiation for each sample position is severely limited by the resulting beam damage, and thus limiting the amount of backscattered electrons that reach the detector. One promising approach has been to reduce

sample degradation of MAPbI₃ during EBSD measurements by using low-vacuum chamber pressures inside the SEM with up to 1 mbar of partial water vapour pressure which reduces charge accumulation on each sample position. In this way, grain orientation mapping with sub-grain resolution of MAPbI₃ thin films was achieved for the first time in 2019 (Leonhard *et al.*, 2019). This allowed for correlation of grain orientation, ferroelectric domain patterns mapped via PFM as well as contact potential measurements via Kelvin Probe Force Microscopy (KPFM). Soon after, using ultrafast EBSD detectors, the resolution of EBSD measurements was further improved, even revealing intra-grain strain in MAPbI₃ thin films (Jariwala *et al.*, 2019). These results show that many established microscale characterization techniques that have been used on ceramic ferroelectrics in the past can also be adapted to OMH perovskites, but the mechanical and chemical instability of these compounds often require adjusted measurement parameters and sometimes even technological improvements.

7.4 Implications of ferroelectricity in light absorbing semiconductors

At this time, it is still not fully understood to what extent the ferroelectric domains in MAPbI₃ solar cells actually have an impact on the solar cell performance. On the one hand, there are simulations and first experimental works suggesting that the formation of ordered alternating lateral domains is beneficial, mainly in order to reduce SRH recombination via spatial separation of electrons and holes within the perovskite grains (Frost *et al.*, 2014; Rossi *et al.*, 2018; Leonhard *et al.*, 2021). On the other hand, perovskite compositions that are likely to possess a cubic and thereby paraelectric crystal structure at room temperature allow for very high solar cell efficiencies very close to the theoretical limits (Yoo *et al.*, 2021; Hui *et al.*, 2021).

One of the biggest challenges for separating the various crystalline, ionic and electronic effects in OMH perovskites is the lack of comparability between different perovskite compositions. There is no way of making a perovskite solar cell with and without ferroelectric properties without changing its crystal structure and often even the thin film morphology. One seemingly obvious approach is to heat a ferroelectric perovskite solar cell beyond T_C and compare the device properties. But even though for example MAPbI₃ solar cells perform worse when heated to the cubic phase, ionic effects and thereby defect densities, shifts of the conduction and valence band energies as well as strain within the thin film could be reasonable explanations besides direct influence from ferroelectric domains (Schwenzer *et al.*, 2018; Zhu *et al.*, 2019). Additionally, both tetragonal and cubic phases can coexist in thin film samples of MAPbI₃ at room temperature and up to 330 K (Whitfield *et al.*, 2016; Kim *et al.*, 2018b; Kim *et al.*, 2018c).

Unlike real experiments, simulations allow comparison of perovskites with identical properties besides crystal polarization and can thereby inform a deeper understanding of charge carrier dynamics. In order to yield meaningful results, the underlying assumptions and parameters must sufficiently reflect the real system. Rossi *et al.* used finite-element discretization of drift-diffusion equations to simulate domain patterns that were previously observed via PFM measurements on MAPbI₃ thin films (Rossi *et al.*, 2018). Fig. 7.9 shows three different variations of ferroelectric domains, electron and hole densities along laterally cut planes, and the respective spatial SRH recombination rates. These simulations showed that specific ferroelectric domain configurations could affect recombination losses, particularly in thin films with high defect mediated trap-densities. Generally, the formation of lateral 90° domains with charged domain walls was predicted to have the most beneficial

impact on device performance while uncharged domain walls are less likely to affect the solar cell. Vertical polarization components (perpendicular to the planar electrodes) do not affect charge carrier recombination rates but they might affect ionic charge carrier densities and thereby the surface potentials at the interfaces towards neighbouring charge transport layers or electrodes. This effect could be utilized by applying vertical poling to solar cells in order to improve directional charge carrier transport and charge carrier extraction in unoptimized solar cell stacks as was previously demonstrated on the ferroelectric oxides $\text{Bi}_2\text{FeCrO}_6$ and KNN-BNNO (Ba and Ni doped $(\text{K},\text{Na})\text{NbO}_3$) (Nechache *et al.*, 2015; Bai *et al.*, 2018).

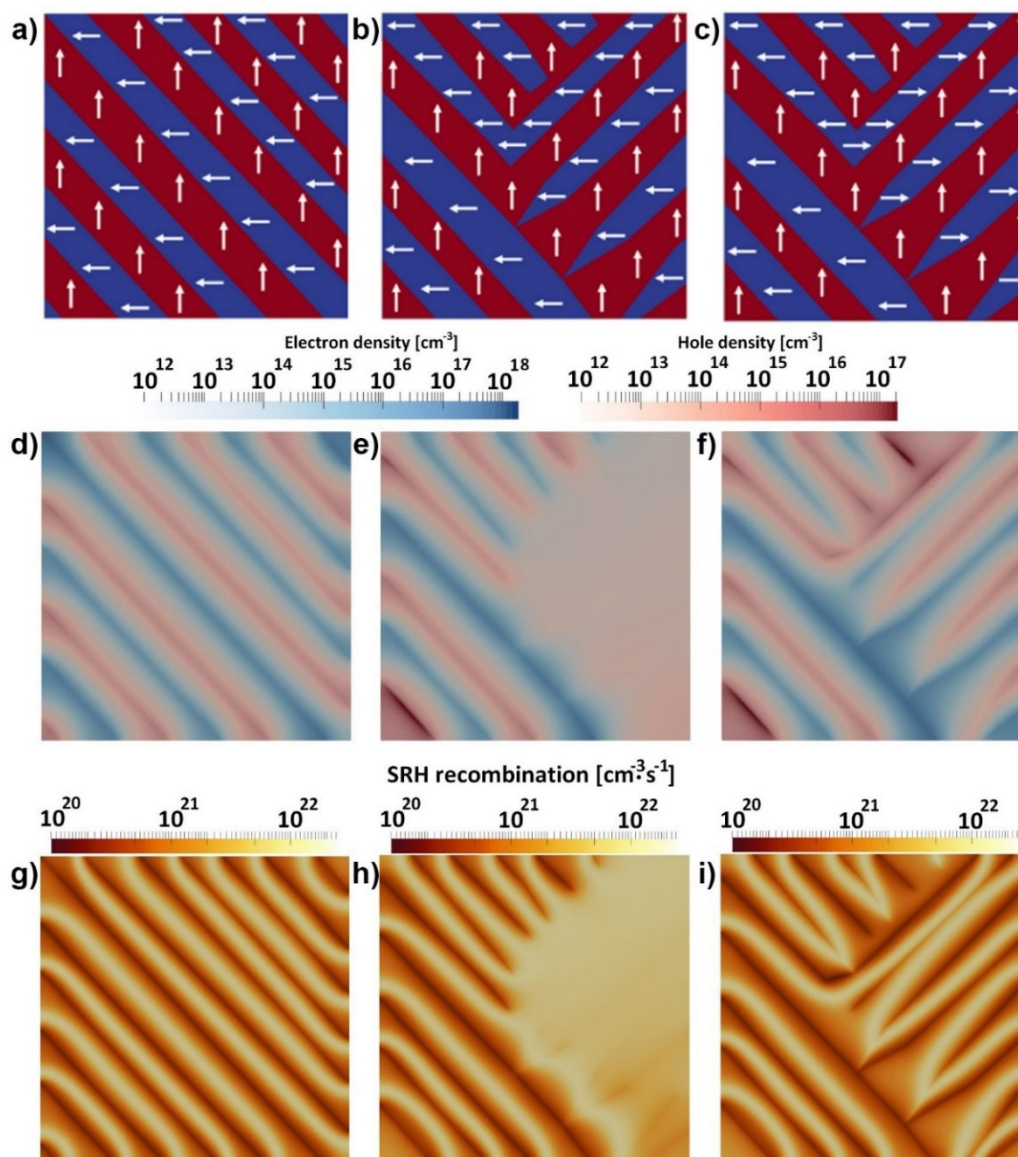


Figure 7.9. (a-c) Various models of lateral ferroelectric domain polarization patterns based on PFM measurements of MAPbI₃ thin films. (d-e) Drift-Diffusion simulations of charge carrier densities during illumination of the modelled solar cell reveal separate areas of higher electron- or hole-densities in lateral cut planes of the crystal grain even for a moderate polarization of 0.2 $\mu\text{C}/\text{cm}^2$. (g-i) The resulting SRH recombination rate is significantly reduced in areas of the lowest overlap between electron- and hole-densities. (Adapted with permission from: Rossi *et al.*, 2018.)

Although simulations have shown that some domain configurations of a semiconducting ferroelectric light absorbing material could reduce SRH-recombination losses, generally,

ferroelectricity could also have detrimental effects on perovskite solar cells (Frost *et al.*, 2014; Rossi *et al.*, 2018). In particular, perovskite compositions that have a T_C within the operational range of solar cells will likely go through this transition when the solar cell heats up or cools down due to sun illumination in the morning, sunset in the evening and varying weather conditions. This is the case for many OMH perovskites, e.g., MAPbI_3 ($T_C \sim 55^\circ\text{C}$) and $\text{FA}_{0.1}\text{MA}_{0.9}\text{PbI}_3$ ($T_C \sim 25^\circ\text{C}$) (Francisco-López *et al.*, 2020). A ferroelectric to paraelectric phase transition always coincides with the release of screening charges at domain walls which could severely impact compositional stability in a material like MAPbI_3 that possesses a low activation energy for its A- and X-site ions (MA^+ , I). Repeated trapping and release of these ions at domain walls could mediate crystal decomposition or severely change its electronic properties (Colsmann *et al.*, 2019). A similar process might occur at domain walls whenever a ferroelectric OMH perovskite is exposed to illumination. At this point it is still unclear whether screening charges at domain walls mainly comprise ionic or electronic charge carriers but, it seems plausible that in dark conditions these screening charges are predominantly ionic, since previously photogenerated free electronic charges (electrons and holes) are likely to recombine and the remaining thermally activated electron and hole densities are much lower. Therefore, a MAPbI_3 sample might release ionic charge carriers from domain walls, once an abundance of electrons and holes are generated under illumination that can hence contribute to domain polarization screening. Conversely, when illumination is removed, ionic charges are more likely to get trapped at domain walls until the polarization is screened. These processes might contribute to the slow time constants and capacitive effects that are often observed in solar simulator or External Quantum Efficiency (EQE) measurements in perovskite solar cells (Ravishankar *et al.*, 2018; Röhm, 2018).

Additionally, crossing the tetragonal to cubic phase transition temperature will lead to fluctuations of stress and hence will result in strain within the perovskite thin film. These repetitive changes in strain could not only lead to defect formation and changes of the interfaces between perovskite grains and surrounding charge transport layers in a solar cell, but this will likely also impact grain morphology and properties of grain boundaries over time. These effects might even be one of the crucial limiting factors to the long-term stability of some OMH-perovskite compositions. Besides device stability, tensile strain in OMH solar cells can also directly or indirectly change electronic properties and thereby impact solar cell performance (Zhu *et al.*, 2019). Besides temperature effects around the phase transition in a light-absorbing perovskite thin film, electric fields might play a role when the material is ferroelectric. Both during solar cell operation and device testing, electric fields on the order of 1-10 $\text{V}/\mu\text{m}$ can occur within the perovskite film depending on the layer thickness, illumination intensity and external bias. As discussed in the previous sections of this chapter, ferroelectric domains in MAPbI_3 are affected by electric fields of this magnitude if they are applied for several minutes. Whether or not ferroelectric poling occurs depends on strain constraints (clamping, pinning, tetragonality), the alignment of the electric field relative to the crystal polarization, and the temperature. This potential for creeping poling in ferroelectric OMH-perovskite solar cells seems very likely to mediate changes to electronic properties and to impact device stability over time.

7.5 What is next for metal halide perovskites?

Metal halide perovskites are currently at the crossroads where several pioneering companies have started to commercialize their products, but it is still unclear which markets will become most feasible. Will the tandem approach bring sufficient improvements to the efficiency of

solar modules by harvesting high-energy photons with a perovskite solar cell on top of a regular silicon solar cell? Can the lifetime of the metal halide perovskite devices match the excellent lifetimes of silicon solar cells that already exceed 30 years? Or will perovskite solar cells by themselves cross the barrier of becoming competitive with silicon solar cells by outcompeting them in terms of production cost? If these scenarios do not come to fruition, it will most likely be due to limitations of stability of the perovskite crystals or the currently still unavoidable incorporation of the heavy metal lead.

Intrinsic material properties like ferroelectricity, ferroelasticity and phase transitions will play a pivotal role not only in understanding the photophysics and charge carrier dynamics in perovskite solar cells but also in improving the currently used perovskite compositions in terms of stability and power conversion efficiency. Development of lead-free alternative materials with similar properties will certainly require a good understanding of all the physical processes in the crystal under illumination. The same holds true for other applications of this fascinating material class such as perovskite-LEDs, perovskite photodetectors or perovskite electronics. Whether ferroelectricity turns out to be beneficial or detrimental to perovskite charge carrier generation, charge carrier transport and recombination dynamics, it certainly will be a key parameter to optimize. Most state-of-the-art OMH perovskite compositions comprise tetragonal to cubic phase transitions within the solar cells' operational temperature range, but these devices are most often only optimized for standard testing conditions (e.g. 25°C) and it is still unclear whether these properties are sustained at higher or lower operation conditions that can entail a different crystal phase. Understanding and controlling these phase transitions will certainly play an important role in improving the long-term stability and average power conversion efficiencies of perovskite solar cells outside today's research labs.

References

- Bai et al., 2018 Bai, Y., Vats, G., Seidel, J., Jantunen, H., Juuti, J. (2018) Boosting Photovoltaic Output of Ferroelectric Ceramics by Optoelectric Control of Domains, *Adv. Mater.*, 30(43), 1803821
- Breternitz et al., 2019 Breternitz, J., Lehmann, F., Barnett, S. A., Nowell, H., Schorr, S. (2019) Role of the Iodide–Methylammonium Interaction in the Ferroelectricity of CH₃NH₃PbI₃, *Angew. Chem. Int. Ed.*, 59(1), pp. 424-428
- Breternitz et al., 2020 Breternitz, J., Tovar, M., Schorr, S. (2020) Twinning in MAPbI₃ at room temperature uncovered through Laue neutron diffraction, *Sci. Rep.*, 10, 16613
- Chao et al., 2018 Chao, L., Wang, Z., Xia, Y., Chen, Y., Huang, W. (2018) Recent progress on low dimensional perovskite solar cells, *J. Energy Chem.*, 27(4), pp. 1091-1100
- Chen et al., 2021 Chen, J., He, D., Park, N.-G. (2021) Methodologies for >30% Efficient Perovskite Solar Cells via Enhancement of Voltage and Fill Factor, *Solar RRL*, 6(1), 2100767
- Collins et al., 2019 Collins, L., Liu, Y., Ovchinnikova, O. S., Proksch, R. (2019) Quantitative Electromechanical Atomic Force Microscopy, *ACS Nano*, 13(7), pp. 8055-8066
- Colsmann et al., 2019 Colsmann, A., Röhm, H. (2019) Ferroelectricity and stability measurements in perovskite solar cells, *J. Phys. Energy*, 2, 011003

- Colsmann et al., 2020 Colsmann, A., Leonhard, T., Schulz, A. D., Röhm, H. (2020) Comment on “ferroelectricity-free lead halide perovskites” by A. Gómez et al., *Energy Environ. Sci.*, 13, pp. 1888-1891
- Fan et al., 2015 Fan, Z., Xiao, J., Sun, K., Chen, L., Hu, Y., Ouyang, J., Ong, K. P., Zeng, K., Wang, J. (2015) Ferroelectricity of CH₃NH₃PbI₃ Perovskite, *J. Phys. Chem. Lett.*, 6(7), pp. 1155-1161
- Feng, 2014 Feng, J. (2014) Mechanical properties of hybrid organic-inorganic CH₃NH₃BX₃ (B = Sn, Pb; X = Br, I) perovskites for solar cell absorbers, *APL Mater.*, 2, 081801
- Francisco-López et al., 2020 Francisco-López, A., Charles, B., Alonso, M. I., Garriga, M., Campoy-Quiles, M., Weller, M. T., Goñi, A. R. (2020) Phase Diagram of Methylammonium/Formamidinium Lead Iodide Perovskite Solid Solutions from Temperature-Dependent Photoluminescence and Raman Spectroscopies, *J. Phys. Chem. C*, 124(6), pp. 3448-3458
- Frost and Walsh, 2016 Frost, J. M. and Walsh, A. (2016) What Is Moving in Hybrid Halide Perovskite Solar Cells?, *Acc. Chem. Res.*, 49(3), pp. 528-535
- Frost et al., 2014 Frost, J. M., Butler, K. T., Brivio, F., Hendon, C. H., van Schilfgaarde, M., Walsh, A. (2014) Atomistic Origins of High-Performance in Hybrid Halide Perovskite Solar Cells, *Nano Lett.*, 14(5), pp. 2584-2590
- Futscher et al., 2019 Futscher, M. H., Lee, J. M., McGovern, L., Muscarella, L. A., Wang, T., Haider, M. I., Fakharuddin, A., Schmidt-Mende, L., Ehrler, B. (2019) Quantification of ion migration in CH₃NH₃PbI₃ perovskite solar cells by transient capacitance measurements, *Mater. Horiz.*, 6, pp. 1497-1503
- Gomez et al., 2020 Gomez, A., Wang, Q., Goñi, A. R., Campoy-Quiles, M., Abate, A. (2020) Reply to the “Comment on the publication ‘Ferroelectricity-free lead halide perovskites’ by Gomez et al.” by Colsmann et al., *Energy Environ. Sci.*, 13, pp. 1892-1895
- Green et al., 2014 Green, M. A., Ho-Baillie, A., Snaith, H. J. (2014) The emergence of perovskite solar cells, *Nat. Photonics*, 8, pp. 506-514
- Hermes et al., 2016 Hermes, I. M., Bretschneider, S. A., Bergmann, V. W., Li, D., Klasen, A., Mars, J., Tremel, W., Laquai, F., Butt, H.-J., Mezger, M., Berger, R., Rodriguez, B. J., Weber, S. A. L. (2016) Ferroelastic Fingerprints in Methylammonium Lead Iodide Perovskite, *J. Phys. Chem. C*, 120(10), pp. 5724-5731
- Hieulle et al., 2017 Hieulle, J., Stecker, C., Ohmann, R., Ono, L. K., Qi, Y. (2017) Scanning Probe Microscopy Applied to Organic-Inorganic Halide Perovskite Materials and Solar Cells, *small methods*, 2(1), 1700295
- Hsieh et al., 2017 Hsieh, C.-M., Yu, Y.-L., Chen, C.-P., Chuang, S.-C. (2017) , Effects of the additives n-propylammonium or n-butylammonium iodide on the performance of perovskite solar cells, *RSC Adv.*, 7, pp. 55986-55992
- Hui et al., 2021 Hui, W., Chao, L., Lu, H., Xia, Q., Su, Z., Niu, T., Tao, L., Du, B., Li, D., Wang, Y., Dong, H., Zuo, S., Li, B., Shi, W., Ran, X., Li, P., Zhang, H., Wu, Z., Ran, C., Song, L., Xing, G., Gao, X., Zhang, J., Xia, Y., Chen, Y., Huang, W. (2021) Stabilizing black-phase formamidinium perovskite formation at room temperature and high humidity, *Science*, 371(6536), pp. 1359-1364
- Jariwala et al., 2019 Jariwala, S., Sun, H., Adhyaksa, G. W. P., Lof, A., Muscarella, L. A., Ehrler, B., Garnett, E. C., Ginger, D. S. (2019) Local Crystal Misorientation Influences Non-radiative Recombination in Halide Perovskites, *Joule*, 3(12), pp. 3048-3060
- Kim et al., 2012 Kim, H.-S., Lee, C.-R., Im, J.-H., Lee, K.-B., Moehl, T., Marchioro, A., Moon, S.-J., Humphry-Baker, R., Yum, J.-H., Moser, J. E., Grätzel, M., Park, N.-G. (2012) Lead Iodide Perovskite Sensitized All-Solid-State

- Submicron Thin Film Mesoscopic Solar Cell with Efficiency Exceeding 9%, *Sci. Rep.*, 2, 591
- Kim et al., 2018a Kim, T. W., Shibayama, N., Cojocar, L., Uchida, S., Kondo, T., Segawa, H. (2018) Real-Time In Situ Observation of Microstructural Change in Organometal Halide Perovskite Induced by Thermal Degradation, *Adv. Funct. Mater.*, 28(42), 1804039
- Kim et al., 2018b Kim, T. W., Uchida, S., Matsushita, T., Cojocar, L., Jono, R., Kimura, K., Matsubara, D., Shirai, M., Ito, K., Matsumoto, H., Kondo, T., Segawa, H. (2018) Self-Organized Superlattice and Phase Coexistence inside Thin Film Organometal Halide Perovskite, *Adv. Mater.*, 30(8), 1705230
- Kim et al., 2018c Kim, T. W., Matsushita, T., Uchida, S., Kondo, T., Segawa, H. (2018) Quantitative fraction analysis of coexisting phases in a polycrystalline CH₃NH₃PbI₃ perovskite, *Appl. Phys. Express*, 11, 101401
- Kojima et al., 2006 Kojima, A., Teshima, K., Miyasaka, T., Shirai, Y. (2006) Novel Photoelectrochemical Cell with Mesoscopic Electrodes Sensitized by Lead-Halide Compounds (2), *Meet. Abstr.*, MA2006-02, 397
- Kutes et al., 2014 Kutes, Y., Ye, L., Zhou, Y., Pang, S., Huey, B. D., Padture, N. P. (2014) Direct Observation of Ferroelectric Domains in Solution-Processed CH₃NH₃PbI₃ Perovskite Thin Films, *J. Phys. Chem. Lett.*, 5(19), pp. 3335-3339
- Lee et al., 2012 Lee, M. M., Teuscher, J., Miyasaka, T., Murakami, T. N., Snaith, H. J. (2012) Efficient Hybrid Solar Cells Based on Meso-Superstructured Organometal Halide Perovskites, *Science*, 338(6107), pp. 643-647
- Leguy et al., 2015 Leguy, A. M. A., Frost, J. M., McMahon, A. P., Sakai, V. G., Kockelmann, W., Law, C. H., Li, X., Foglia, F., Walsh, A., O'Regan, B. C., Nelson, J., Cabral, J. T., Barnes, P. R. F. (2015) The dynamics of methylammonium ions in hybrid organic-inorganic perovskite solar cells, *Nat. Comm.*, 6, 7124
- Leonhard et al., 2019 Leonhard, T., Schulz, A. D., Röhm, H., Wagner, S., Altermann, F. J., Rheinheimer, W., Hoffmann, M. J., Colmann, A. (2019) Probing the Microstructure of Methylammonium Lead Iodide Perovskite Solar Cells, *Energy Technol.*, 7(3), 1800989
- Leonhard et al., 2021 Leonhard, T., Röhm, H., Altermann, F. J., Hoffmann, M. J., Colmann, A. (2021) Evolution of ferroelectric domains in methylammonium lead iodide and correlation with the performance of perovskite solar cells, *J. Mater. Chem. A*, 9, pp. 21845-21858
- Li et al., 2019 Li, X., Fu, S., Liu, S., Wu, Y., Zhang, W., Song, W., Fang, J. (2019) Suppressing the ions-induced degradation for operationally stable perovskite solar cells, *Nano Energy*, 64, 103962
- Liu et al., 2018 Liu, Y., Collins, L., Proksch, R., Kim, S., Watson, B. R., Doughty, B., Calhoun, T. R., Ahmadi, M., Ievlev, A. V., Jesse, S., Retterer, S. T., Belianinov, A., Xiao, K., Huang, J., Sumpter, B. G., Kalinin, S. V., Hu, B., Ovchinnikova, O. S. (2018) Chemical nature of ferroelastic twin domains in CH₃NH₃PbI₃ perovskite, *Nat. Mater.*, 17, pp. 1013-1019
- Liu et al., 2019 Liu, Y., Collins, L., Proksch, R., Kim, S., Watson, B. R., Doughty, B., Calhoun, T. R., Ahmadi, M., Ievlev, A. V., Jesse, S., Retterer, S. T., Belianinov, A., Xiao, K., Huang, J., Sumpter, B. G., Kalinin, S. V., Hu, B., Ovchinnikova, O. S. (2019) Reply to: On the ferroelectricity of CH₃NH₃PbI₃ perovskites, *Nat. Mater.*, 18, pp. 1051-1053
- Nechache et al., 2015 Nechache, R., Harnagea, C., Li, S., Cardenas, L., Huang, W., Chakrabarty, J., Rosei, F. (2015) Bandgap tuning of multiferroic oxide solar cells, *Nat. Photon.*, 9, pp. 61-67

- Ono et al., 2019 Ono, L. K., Liu, S. (F.), Qi, Y. (2019) Reducing Detrimental Defects for High-Performance Metal Halide Perovskite Solar Cells, *Angew. Chem. Int. Ed.*, 59(17), pp. 6676-6698
- Pecchia et al., 2015 Pecchia, A., Gentilini, D., Rossi, D., Auf der Maur, M., Di Carlo, A. (2015) Role of Ferroelectric Nanodomains in the Transport Properties of Perovskite Solar Cells, *Nano Lett.*, 16(2), pp. 988-992
- Poglitsch and Weber, 1987 Poglitsch, A. and Weber, D. (1987) Dynamic disorder in methylammoniumtrihalogenoplumbates (II) observed by millimeter-wave spectroscopy, *J. Chem. Phys.*, 87, 6373
- Rakita et al, 2017 Rakita, Y., Bar-Elli, O., Meirzadeh, E., Kaslasi, H., Peleg, Y., Hodes, G., Lubomirsky, I., Oron, D., Ehre, D., Cahen, D. (2017) Tetragonal CH₃NH₃PbI₃ is ferroelectric, *Proc. Natl. Acad. Sci.*, 114(28), pp. E5504-E5512
- Ravishankar et al., 2018 Ravishankar, S., Aranda, C., Boix, P., Anta, J. A., Bisquert, J., Garcia-Belmonte, G. (2018) Effects of Frequency Dependence of the External Quantum Efficiency of Perovskite Solar Cells, *J. Phys. Chem. Lett.*, 9(11), pp. 3099-3104
- Richter et al., 2018 Richter, C., Zschornak, M., Novikov, D., Mehner, E., Nentwich, M., Hanzig, J., Gorfman, S., Meyer, D. C. (2018) Picometer polar atomic displacements in strontium titanate determined by resonant X-ray diffraction, *Nat. Comm.*, 9, 178
- Röhm et al., 2017 Röhm, H., Leonhard, T., Hoffmann, M. J., Colsmann, A. (2017) Ferroelectric domains in methylammonium lead iodide perovskite thin-films, *Energy Environ. Sci.*, 10, pp. 950-955
- Röhm et al., 2019 Röhm, H., Leonhard, T., Hoffmann, M. J., Colsmann, A. (2019) Ferroelectric Poling of Methylammonium Lead Iodide Thin Films, *Adv. Funct. Mater.*, 30(5), 1908657
- Röhm, 2019 Röhm, H. (2019) Ferroelektrizität in Methylammoniumbleiiodid-Solarzellen, PhD thesis, Karlsruhe Institute of Technology, Karlsruhe
- Rossi et al., 2018 Rossi, D., Pecchia, A., Auf der Maur, M., Leonhard, T., Röhm, H., Hoffmann, M. J., Colsmann, A., Di Carlo, A. (2018) On the importance of ferroelectric domains for the performance of perovskite solar cells, *Nano Energy*, 48, pp. 20-26
- Rothmann et al., 2017a Rothmann, M. U., Li, W., Etheridge, J., Cheng, Y.-B. (2017) Microstructural Characterisations of Perovskite Solar Cells – From Grains to Interfaces: Techniques, Features, and Challenges, *Adv. Energy Mater.*, 7(23), 1700912
- Rothmann et al., 2017b Rothmann, M. U., Li, W., Zhu, Y., Bach, U., Spiccia, L., Etheridge, J., Cheng, Y.-B. (2017) Direct observation of intrinsic twin domains in tetragonal CH₃NH₃PbI₃, *Nat. Comm.*, 8, 14547
- Saliba et al., 2015 Saliba, M., Matsui, T., Seo, J.-Y., Domanski, K., Correa-Baena, J.-P., Nazeeruddin, M. K., Zakeeruddin, S. M., Tress, W., Abate, A., Hagfeldt, A., Grätzel, M. (2016) Cesium-containing triple cation perovskite solar cells: improved stability, reproducibility and high efficiency, *Energy Environ. Sci.*, 9, pp. 1989-1997
- Schulz et al., 2019 Schulz, A. D., Röhm, H., Leonhard, T., Wagner, S., Hoffmann, M. J., Colsmann, A. (2019) On the ferroelectricity of CH₃NH₃PbI₃ perovskites, *Nat. Mater.*, 18, p. 1050
- Schwenzer et al., 2018 Schwenzer, J., Rakocevic, L., Gehlhaar, R., Abzieher, T., Gharibzadeh, S., Moghadamzadeh, S., Quintilla, A., Richards, B. S., Lemmer, U., Paetzold, U. (2018) Temperature Variation-Induced Performance Decline of Perovskite Solar Cells, *ACS Appl. Mater. Interfaces*, 10(19), pp. 16390-16399

- Sun et al., 2017 Sun, S., Isikgor, F. H., Deng, Z., Wei, F., Kieslich, G., Bristowe, P. D., Ouyang, J., Cheetham, A. K. (2017) Factors Influencing the Mechanical Properties of Formamidinium Lead Halides and Related Hybrid Perovskites, *ChemSusChem*, 10(19), pp. 3740-3745
- Tai et al., 2019 Tai, Q., Tang, K.-C., Yan, F. (2019) Recent progress of inorganic perovskite solar cells, *Energy Environ. Sci.*, 12, pp. 2375-2405
- Tao et al., 2019 Tao, S., Schmidt, I., Brocks, G., Jiang, J., Tranca, I., Meerholz, K., Olthof, S. (2019) Absolute energy level positions in tin- and lead-based halide perovskites, *Nat. Comm.*, 10, 2560
- Veldhuis et al., 2016 Veldhuis, S. A., Boix, P. P., Yantara, N., Li, M., Sum, T. C., Mathews, N., Mhaisalkar, S. G. (2016) Perovskite Materials for Light-Emitting Diodes and Lasers, *Adv. Mater.*, 28(32), pp. 6804-6834
- Wang et al., 2017a Wang, Z., Lin, Q., Chmiel, F. P., Sakai, N., Herz, L. M., Snaith, H. J. (2017) Efficient ambient-air-stable solar cells with 2D–3D heterostructured butylammonium-caesium-formamidinium lead halide perovskites, *Nat. Energy*, 2, 17135
- Wang et al., 2017b Wang, H.-C., Bao, Z., Tsai, H.-Y., Tang, A.-C., Liu, R.-S. (2017) Perovskite Quantum Dots and Their Application in Light-Emitting Diodes, *small*, 14(1), 1702433
- Wang et al., 2018 Wang, F., Bai, S., Tress, W., Hagfeldt, A., Gao, F. (2018) Defects engineering for high-performance perovskite solar cells, *npj Flex. Electron.*, 2, 22
- Weber et al., 2018 Weber, S. A. L., Hermes, I. M., Turren-Cruz, S.-H., Gort, C., Bergmann, V. W., Gilson, L., Hagfeldt, A., Graetzel, M., Tress, W., Berger, R. (2018) How the formation of interfacial charge causes hysteresis in perovskite solar cells, *Energy Environ. Sci.*, 11, pp. 2404-2413
- Wei and Huang, 2019 Wei, H. and Huang J. (2019) Halide lead perovskites for ionizing radiation detection, *Nat. Comm.*, 10, 1066
- Wei et al., 2014 Wei, J., Zhao, Y., Li, H., Li, G., Pan, J., Xu, D., Zhao, Q., Yu, D. (2014) Hysteresis Analysis Based on the Ferroelectric Effect in Hybrid Perovskite Solar Cells, *J. Phys. Chem. Lett.*, 5(21), pp. 3937-3945
- Whitfield et al., 2016 Whitfield, P. S., Herron, N., Guise, W. E., Page, K., Cheng, Y. O., Milas, I., Crawford, M. K. (2016) Structures, Phase Transitions and Tricritical Behavior of the Hybrid Perovskite Methyl Ammonium Lead Iodide, *Sci. Rep.*, 6, 35685
- Wilson et al., 2019 Wilson, J. N., Frost, J. M., Wallace, S. K., Walsh, A. (2019) Dielectric and ferroic properties of metal halide perovskites, *APL Mater.*, 7, 010901
- Wu et al., 2018 Wu, H.-T., Chen, Y.-F., Shih, C.-F., Leu, C.-C., Wu, S.-H. (2018) Memory properties of (110) preferring oriented CH₃NH₃PbI₃ perovskite film prepared using PbS-buffered three-step growth method, *Thin Solid Films*, 660, pp. 320-327
- Xiao et al., 2015 Xiao, C., Li, Z., Guthrey, H., Moseley, J., Yang, Y., Wozny, S., Moutinho, H., To, B., Berry, J. J., Gorman, B., Yan, Y., Zhu, K., Al-Jassim, M. (2015) Mechanisms of Electron-Beam-Induced Damage in Perovskite Thin Films Revealed by Cathodoluminescence Spectroscopy, *J. Phys. Chem. C*, 119(48), pp. 26904-26911
- Yoo et al., 2021 Yoo, J. J., Seo, G., Chua, M. R., Park, T. G., Lu, Y., Rotermund, F., Kim, Y.-K., Moon, C. S., Jeon, N. J., Correa-Baena, J.-P., Bulović, V., Shin, S. S., Bawendi, M. G., Seo, J. (2021) Efficient perovskite solar cells via improved carrier management, *Nature*, 590, pp. 587-593
- Zhu et al., 2019 Zhu, C., Niu, X., Fu, Y., Li, N., Hu, C., Chen, Y., He, X., Na, G., Liu, P., Zai, H., Ge, Y., Ke, X., Bai, Y., Yang, S., Chen, P., Li, Y., Sui, M., Zhang, L.,

Zhukov et al., 2010

Zhou, H., Chen, Q. (2019) Strain engineering in perovskite solar cells and its impacts on carrier dynamics, *Nat. Comm.*, 10, 815

Zhukov, S., Fedosov, S., Glaum, J., Granzow, T., Genenko, Y. A., von Seggern, H. (2010) Effect of bipolar electric fatigue on polarization switching in lead-zirconate-titanate ceramics, *J. Appl. Phys.*, 108, 014105